Supporting Information:

Direct Evidence of Conformational Changes Associated with Voltage-Gating in a Voltage Sensor Protein by Time-Resolved X-ray/Neutron Interferometry.

A. Tronin[1], C.E. Nordgren,[1] J.W. Strzalka[2], I. Kuzmenko[2], D. Worcester[3], V. Lauter[4], J.A. Freites[5], D.J. Tobias[5] and J.K. Blasie[1]

[1]Department of Chemistry, University of Pennsylvania, Philadelphia, PA 19104
[2]X-ray Science Division, Advanced Photon Source, Argonne National Laboratory, Argonne, IL 60439
[3]Department of Physiology & Biophysics, University of California Irvine, Irvine, CA 92697
[4]Spallation Neutron Source, Oak Ridge National Laboratory, Oak Ridge, TN 37831
[5]Department of Chemistry, University of California Irvine, Irvine, CA 92697

Fabrication of the Reconstituted VSD:POPC Membrane:

Two methods have been described for the preparation of single membranes tethered to the surface of an inorganic substrate, the membrane comprised of a phospholipid bilayer (POPC; 1-palmitoyl-2-oleoyl-sn-glycero-3-phosphocholine) containing the voltage sensing domain (VSD) of the voltage-gated potassium channel from *Arepyrum pernix* KvAP, vectorially-oriented with respect to the normal to the membrane plane at high in-plane surface density [S1]. The vectorial orientation and in-plane density greatly facilitate the characterization of the membrane protein's profile structure utilizing x-ray and neutron reflectivity, enhanced by interferometry [S2-S5]. The first, designated as "Self-Assembly (SA)", utilized the hexahis-tag at the C-terminus of the genetically expressed VSD to bind the detergent (OG: n-octyl-β-D-glucopyranoside) solubilized protein to the nitrilotriacetate endgroups of an organic self-assembled monolayer chemisorbed onto the silicon oxide surface of the inorganic multilayer substrate via nickel coordination chemistry. For this work, the SiGeSi or SiNiSi multilayer substrates were fabricated on a commercial silicon wafer by dc magnetron sputtering and the thickness for each of the sputtered layers was 20Å. The detergent was subsequently exchanged for the phospholipid by incubation with a micellar phospholipid-detergent solution in the presence of Bio-beads possessing a high affinity for the detergent. This SA approach to forming the reconstituted VSD:POPC membrane tethered to the substrate surface is illustrated schematically in Figure S2. The second, designated as "Directed Assembly (DA)", utilized a Langmuir monolayer comprised initially of a mixture of the detergent(OG) solubilized VSD protein and the phospholipid at the water-air interface, that was compressed to a surface pressure at which the x-ray reflectivity from the monolayer indicated that the axis of the 4-helix bundle component of the VSD protein's structure was aligned approximately normal to the interface. BioBeads in the aqueous subphase beneath the Langmuir monolayer effectively removed the detergent from the Langmuir monolayer during its compression, the compressed monolayer retaining the phospholipid and protein. The nitrilotriacetate endgroups of an organic self-assembled monolayer on the silicon oxide surface of the SiGeSi multilayer substrate were then brought into contact with the mixed VSD:POPC Langmuir monolayer from below in the subphase beneath the compressed Langmuir monolayer in the presence of nickel, again to bind the VSD protein to the endgroups via nickel coordination chemistry. The VSD:POPC monolayer attached to the substrate was then incubated with a micellar phospholipid-detergent solution analogous to that used in the SA approach in order to saturate the phospholipid component of the reconstituted membrane. This DA approach is illustrated schematically in Figure S3. Importantly, VSD:POPC membranes formed by both the SA and DA methods were investigated in this work to demonstrate specimen-to-specimen reproducibility.

X-ray and Neutron Interferometry:

The specular x-ray or neutron reflectivity from a thin bio-organic layer at the interface between a uniform solid or liquid substrate and a uniform gas or liquid is relatively weak compared the that from the interface in the absence of the bio-organic layer. Specular reflectivity refers to elastic photon or particle

momentum transfer perpendicular to plane of the interface. Fabricating a nano-scale inorganic multilayer structure on the surface of an inorganic solid substrate, possessing good SLD contrast between the layers, greatly enhances the sensitivity to the presence of the bio-organic layer through the interference of the strong specular reflectivity from the inorganic multilayer with the weaker specular reflectivity form the bio-organic layer on or near its surface. In addition and importantly, this interference effect solves the classic "phase problem" thereby allowing a direct determination of the SLD profile for the bio-inorganic layer, using the known SLD profile of the fabricated multilayer as the key reference structure [S2-S4]. The significance of the x-ray (or neutron) interferometric technique was clearly demonstrated in an earlier publication [S4] via a direct comparison of the x-ray reflectivity from a Langmuir monolayer of an amphiphilic 4-helix bundle protein at the water-air interface *in the absence and presence* of the interferometric effect. The interferometric technique is illustrated with Figures S4 and S5 using this example.

X-ray and Neutron Interferometry Data Analysis as a Function of the Membrane Potential:

We analyzed the x-ray and neutron interferometry data in the first Born approximation, which employs the Fresnel-normalized specular x-ray/neutron reflectivity, $R(Q_z)/R_F(Q_z)$, where $R(Q_z)$ is the experimental specular reflectivity and $R_F(Q_z)$ is the Fresnel function. The Fresnel-normalized reflectivity is proportional to the modulus square of the Fourier transform $F(Q_z)$ of the gradient of the scattering-length density (SLD) profile $d\rho(z)/dz$, where the profile z-axis is normal to the plane of the interfaces(s) comprising the system of interest [S6]. The modulus data, $|F(Q_z)|$, were used in our analysis. The standard errors in these data are expressed in terms of the counting statistics. These errors were propagated through the data reduction procedure, including the footprint correction, the correction for off-specular reflectivity, and division by the Fresnel function for an ideal interface. It is essential to note that this procedure *was precisely the same employing the same parameters*, irrespective of the specimen or the applied potential for each reflectivity technique.

The gradient xSLD or nSLD, $[d\rho(z)/dz]_{0mV}$ or $d\rho_b(z)/dz]_{0mV}$, respectively, for a particular specimen was calculated from its respective modulus data , $|F(Q_z)|$, at 0mV potential utilizing a constrained refinement method to solve the phase problem, the integral of the gradient profile providing the xSLD or nSLD profile itself, $\rho(z, e/Å^3)$ or $\rho_b(z, 10^{-6}/ Å^2)$, as fully described in prior publications [S1, S5]. Two key constraints are utilized, namely the SLD profile of the inorganic multilayer substrate determined independently, and the extent of the SLD profile of the multilayer with the adsorbed bio-organic overlayer determined independently from the autocorrelation of its gradient profile $\{d\rho(z)/dz * d\rho(-z)/dz\}$.

Dropping the distinction between the x-ray and neutron cases, the change in $F(Q_z)$ for either case as a function of the transmembrane potential for any pair of potentials is then $\Delta F(Q_z) = \{F_{pot2}(Q_z) - F_{pot1}(Q_z)\} = \{(\rho_{Si})^{-1} FT [\Delta d\rho(z)/dz\}\}$, where FT denotes the Fourier transform. Since the potential-dependent changes in the modulus data were quite small for all specimens utilized in this investigation, namely less than 3% over the range of Q_z investigated, one can assume that the phase $\varphi(Q_z)$ of $F(Q_z)$ is approximately the same for the two potentials and $\Delta F(Q_z) \sim \{|F_{pot2}(Q_z)| - |F_{pot1}(Q_z)|\} \exp[\varphi(Q_z)]$, as is typical in the analysis of resonance (or "anomalous") x-ray scattering [S7-S8]. As a result, $\Delta|F(Q_z)| = \{|F_{pot2}(Q_z)| - |F_{pot1}(Q_z)|\}$. It is physically reasonable to assume that any potential dependent changes in the profile structure of the inorganic multilayer substrate are negligible, as opposed to those within the profile structure of the bio-organic overlayer. For $\{(\rho_{Si})^{-1} \Delta d\rho(z)/dz\} = FT^{-1} \{\Delta F(Q_z)\}$, the profile extent of $\Delta d\rho(z)/dz$ must be finite and limited to the region of the profile structure containing only the bio-organic overlayer. This extent can be determined from the autocorrelation of $\Delta d\rho(z)/dz$,

namely $\{(\rho_{Si})^{-2} \{\Delta d\rho(z)/dz * \Delta d\rho(-z)/dz\} = FT^{-1}[\Delta|F(Q_z)|]^2 = FT^{-1}\{[|F_{pot2}(Q_z)| - |F_{pot1}(Q_z)|]^2\}$, calculated without the unknown phase information. Since $\Delta d\rho(z)/dz$ must be of finite extent and this is thereby known experimentally, the unknown phase can then be determined via so-called box-refinement

which utilizes only this finite extent as a critical constraint [S6]. The trial structure, whose phase function $\varphi(Q_z)$ was used to initiate the refinement, consisted of a single step-function of uniform non-zero scattering-length density within the interval $10Å < z < 70Å$ and zero otherwise for all potential pairs investigated. This approach, assuming that the small potential-dependent changes in $F(Q_z)$ are dominated by the changes in its modulus, as opposed to its phase, solves the phase problem for the $\Delta \left| F(Q_z) \right|$ data to provide the *difference* gradient SLD profile $\Delta\, d\rho(z)/dz$ to within an overall sign. The unknown overall sign was then simply determined by comparing the modulus of the Fourier transform of $\{[d\rho(z)/dz]_{0mV} \pm[\Delta\, d\rho(z)/dz]_{\pm 100mV}\}$ with its experimental counterpart $\left| F(Q_z) \right|_{\pm 100mV}$, whereupon only one sign was found consistent. The integral of $\{[d\rho(z)/dz]_{0mV} \pm[\Delta\, d\rho(z)/dz]_{\pm 100mV}\}$, using the correct sign, then provides the potential dependence of the profile itself $\rho_{\pm 100mV}(z)$ for the non-zero potentials fully consistent with the key constraint. An example of this approach to determine the potential dependence of $\Delta\, d\rho(z)/dz$ to within an overall sign is illustrated in Figures S6 and S7.

With regard to the method of analysis described above, we make two additional points. First, given the standard errors in the modulus data, $\left| F(Q_z) \right|$, simply deriving the SLD profiles for each value of the potential as described in the second paragraph above results in potential-dependent differences within the inorganic multilayer structure, which are not physically possible. Second, there are other approaches to forcing SLD profile of the inorganic multilayer substrate to be independent of the applied potential. However, the method described above is very effective in the first (and distorted-wave) Born approximations, employing the Fourier transformations noted.

Reproducibility of the Time-Resolved X-ray and Neutron Interferometry Results:

The results from the x-ray experiments for the VSD:POPC membrane were reproducible specimen-to-specimen, as prepared by either "Self-Assembly (SA)" or "Directed Assembly (DA)", and reproducible cycle-to-cycle in the variation of the transmembrane potential over the first two cycles. The results for the hybrid OTS:POPC bilayer, employed as a control lacking the VSD protein in the x-ray experiments, were also reproducible specimen-to-specimen, and reproducible cycle-to-cycle in the variation of the transmembrane potential over the first two cycles. Changes in the nSLD profile of the hybrid bilayer have been described previously [S9], but for only two values of the potential and at much lower spatial resolution than for the xSLD profiles reported here. The structural significance of the potential dependence of the xSLD profiles for the hybrid bilayer is not of any further relevance to this work and will be reported elsewhere. Despite the larger standard errors in the time-resolved neutron experiments, the results for the VSD:POPC membrane were nevertheless also reproducible specimen-to-specimen, as prepared by "Self-Assembly (SA)", and also reproducible for each specimen at two different values of the nSLD contrast provided by the aqueous environment. The results for the SAM employed as the control in the neutron experiments were also reproducible specimen-to-specimen for each specimen at two different values of the nSLD contrast provided by the aqueous environment.

Molecular Dynamics Simulation of a VSD:POPC Membrane as a Function of the Membrane Potential:

Simulation System: The simulation system consisted of one VSD from the *Arepyrum pernix* Kv channel (KvAP) embedded in a bilayer comprised of 232 POPC molecules in excess water (43.3 waters/lipid), and two counterions for a total of 63,247 atoms. The initial configuration of the VSD in the unpolarized and depolarized simulations corresponds to residues 24 to 147 of the KvAP full channel model proposed by Lee et al. [S10]. The initial VSD configuration used in the polarized simulation corresponds to the so-called "down state" model of Schow et al. [S11], which was derived using state-dependent experimental data for the KvAP and *Shaker* channels [S12-S13].

Molecular Dynamics: All-atom, microsecond timescale simulations were performed on Anton, a special-purpose computer for molecular dynamics simulations of biomolecules [S14], using the CHARMM22 [S15] and CHARMM36 [S16] force fields for the protein and lipids, respectively, and the TIP3P model for water [S17]. Simulation algorithms and parameters are described in detail in reference [S18]. The polarized, depolarized and unpolarized trajectories were run for 7 □s, 11 □s, and 5 □s,

respectively. The applied membrane potential in the polarized and depolarized simulations was modeled using a constant electric field, as previously described [S18]. The xSLD and nSLD profiles calculated from the simulations utilized a cylindrical region of the larger simulation system centered on the VSD with the cylinder radius lying in the membrane plane and selected to result in the same lipid to protein mole ratio as the experimental membrane system, namely ~24:1. The *time-averaged* profiles were calculated by averaging over the last 3.7 □s of the unpolarized trajectory and the last 2.5 □s of the polarized and depolarized trajectories.

References:

[S1] Gupta, S., Liu, J., Strzalka, J., and Blasie, J.K. "Profile Structures of the Voltage-sensor Domain and the Voltage-gated K^+-channel Vectorially-oriented in a Single Phospholipid Bilayer Membrane at the Solid-vapor and Solid-liquid Interfaces *via* X-ray Interferometry" *Phys. Rev. E.* 84(3): 031911-1-15.

[S2] Chupa, J.A., McCauley, J.P. Jr., Strongin, R.M., Smith, A.B. III, Blasie, J.K., Peticolas, L.J. and Bean, J.C., Vectorially Oriented Membrane Protein Monolayers: Profile Structures via X-ray Interferometry/Holography. *Biophys. J.* **67**, 336-348 (1994).

[S3] Kneller, L.R., Edwards, A.M., Majkrzak, C.F., Berk, N.F., Krueger, S. and Blasie, J.K., Hydration State of a Single Cytochrome c Monolayer Vectorially-Oriented at a Soft Interface Investigated via Neutron Interferometry. *Biophys. J.* 80(5): 2248-2261 (2001).

[S4] Krishnan, V., Strzalka, J., Liu, J., Liu, C., Kuzmenko, I., Gog, T. and Blasie, J.K., Interferometric Enhancement of X-ray Reflectivity from Unperturbed Langmuir Monolayers of Amphiphiles at the Liquid-Gas Interface. *Phys. Rev. E* 81: 021604-1-10 (2010).

[S5] Gupta, S., Dura, J., Freites, A. Tobias, D. and Blasie, J.K. (2012) Structural Characterization of the Voltage Sensor Domain and Voltage-Gated K^+-Channel Proteins Vectorially-Oriented within a Single Bilayer Membrane at the Solid/Vapor and Solid/Liquid Interfaces *via* Neutron Interferometry. *Langmuir* 28(28):10504-10520.

[S6] Blasie, J.K., Strzalka, J. and Zheng, S. (2003) Solution to the Phase Problem for Specular X-ray & Neutron Reflectivity from Thin Films on Liquid Surfaces. *Phys. Rev. B* 67: 224201-1--224201-8.

[S7] Ramasesahn, S. The Use of Anomalous Scattering in Crystal Structure Analysis, in Advanced Methods in Crystallography, 3ed. G.N. Ramachandran, Academic Press, New York 1964.

[S8] Asturias, F. J. and Blasie, J. K. (1991) Location of the High-Affinity Metal Binding Sites in the Profile Structure of the Ca^{2+}-ATPase of the Sarcoplasmic Reticulum by Resonance X-ray Diffraction. *Biophys. J.* 59:488-502.

[S9] Tronin, A., Chen, C-H., Gupta, S., Worcester, D., Lauter, V., Strzalka, J., Kuzmenko, I. and Blasie, J.K., Structural Changes in Single Membranes in Response to an Applied Transmembrane Electric Potential Revealed by Time-Resolved Neutron/X-ray Interferometry. *Chem. Phys.* 422: 283-289 (2013).

[S10] Lee, S.-Y., Lee, A., Chen, J. and MacKinnon, R., Structure of the KvAP Voltage-dependent K^+ Channel and its Dependence on the Lipid Membrane. *Proc. Nat. Acad. Soc.* **102**, 15441-15446 (2005).

[S11] Schow, E.V., Freites, J.A., Gogna, K., White, S.H. and Tobias, D.J., Down-State Model of the Voltage-Sensing Domain of a Potassium Channel. *Biophys. J.* 98:2857-2866 (2010).

[S12] Ruta, V., Chen, J. and MacKinnon, R., Calibrated Measurment of Gating-Charge Arginine Displacement in the KvAP Voltage-Dependent K^+ Channel, *Cell* 123: 463-475 (2005).

[S13] Tombola, F., Pathak, M.M., Gorostiza, P. and Isacoff, E.Y., The Twisted Ion-Permeation Pathway of a Resting Voltage-Sensing Domain. *Nature* 445(7127):546-549 (2007).

[S14] Shaw, D. E., M. M. Deneroff, R. O. Dror, J. S. Kuskin, R. H. Larson, J. K. Salmon, C. Young, B. Batson, K. J. Bowers, J. C. Chao, M. P. Eastwood, J. Gagliardo, J. P. Grossman, C. R. Ho, D. J. Lerardi, I. Kolossváry, J. L. Klepeis, T. Layman, C. McLeavey, M. A. Moraes, R. Mueller, E. C. Priest, Y. Shan, J. Spengler, M. Theobald, B. Towles, and S. C. Wang, Anton, A Special-purpose Machine for Molecular Dynamics Simulation. *Proc. 34th Annu. Internat. Sym. Computer Architect.* (2007)

[S15] MacKerell, A. D., Jr., M. Feig, and C. L. Brooks, II. Extending the treatment of backbone energetics in protein force fields: Limitations of gas-phase quantum mechanics in reproducing conformational distributions in molecular dynamics simulations. *J. Comput. Chem.* 25:1400-1415 (2004)

[S16] Klauda, J. B., R. M. Venable, J. A. Freites, J. W. O'Connor, D. J. Tobias, C. Mondragon-Ramirez, I. Vorobyov, A. D. MacKerell, Jr., and R. W. Pastor. Update of the CHARMM all-atom additive force field for lipids: validation on six lipid types. *J. Phys. Chem. B* 114:7830-7843 (2010)

[S17] Jorgensen, W. L.; Chandrasekhar, J.; Madura, J. D.; Impey, R. W.; Klein, M. L. Comparison of simple potential functions for simulating liquid water *J.Chem.Phys.* 79:926-935 (1983)

[S18] Freites, J.A., Schow, E.V., White, S.H. and Tobias, D.J., Microscopic Origin of Gating Current Fluctuations in a Potassium Channel Voltage Sensor, *Biophys. J.* 102: L44-L46 (2012).

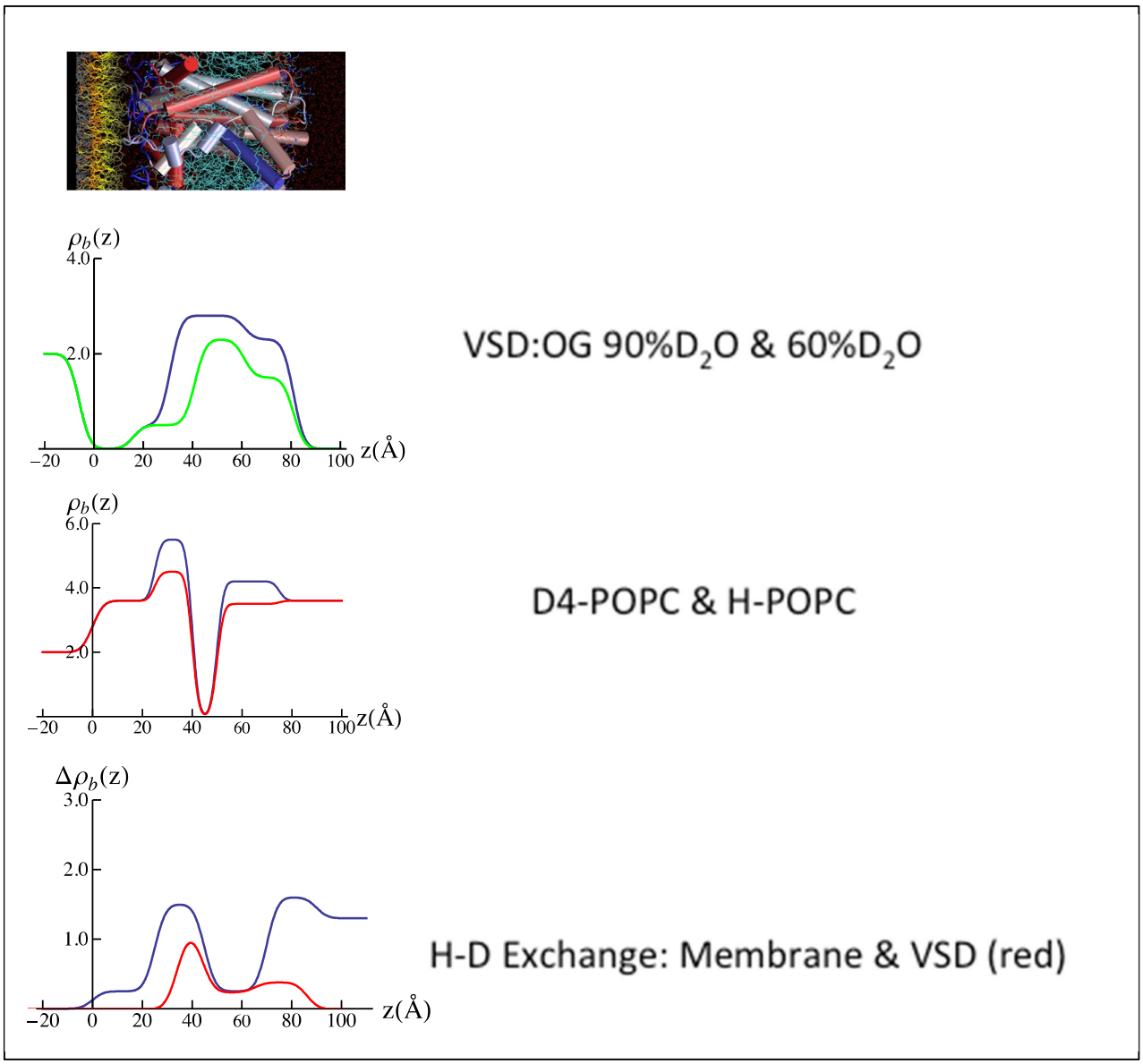

Figure S1: Summary of key results from neutron interferometry adapted from reference [19]. All nSLD profiles shown here are the equivalent "slab-model" representations of their respective Fourier representations derived directly from the Fresnel-normalized specular reflectivity data, as described in reference [S5]. Note that the profiles for the VSD protein (second panel) and H-D exchange profile for the VSD itself (bottom panel, red) have been shifted slightly relative to the profiles for the POPC bilayer within the reconstituted VSD:POPC membrane (third panel) by $\Delta z \sim 5$Å to allow for the slightly different positions of the VSD:OG monolayer and VSD:POPC membrane with respect to the substrate surface.
Top panel: One VSD molecule within the small 3x3 ensemble from Figure 1 is shown to scale in the top panel above the various nSLD profiles shown in the panels below for reference.
Second Panel: The nSLD profiles of only the VSD:OG complex tethered to the surface of the SiNiGe substrate, whose nSLD profile (not shown) occurs for $z < 0$Å with its surface at z=0Å, when hydrated with 90% D_2O/10% H_2O (blue) *versus* with 60% D_2O/40% H_2O (green). Note that water-containing slabs at either surface of the membrane have been removed to reveal the VSD itself (on the surface proximal to the substrate, this slab also includes the chains tethering the VSD to the substrate's surface). The

difference between these two nSLD profiles arises from H-D exchange within, as well as water penetration of, the VSD protein.
Third Panel: The nSLD profiles of the POPC bilayer within the reconstituted VSD:POPC membrane hydrated with 60% D_2O/40% H_2O for fully-hydrogenated POPC (red) and POPC with the two methylene groups of the choline headgroup deuterated (blue), with the water slabs at either surface of the membrane included (on the surface proximal to the substrate, this slab also includes the chains tethering the VSD to the substrate's surface). The difference between these two nSLD profiles arises from the distribution of POPC polar headgroups within the strongly asymmetric bilayer filling the space between adjacent VSD molecules within the membrane plane.
Bottom Panel: The nSLD profiles for H-D exchange within the VSD protein in the membrane (red), namely the difference of the profiles shown in the second panel, with the total H-D exchange for the VSD:POPC membrane (blue). With regard to the latter (blue) profile, there is minimal exchange with the monolayer of chains tethering the VSD molecules to the inorganic surface contained within $0Å < z < 20Å$ in the profiles. Exchange within the layer containing the polar headgroups of the POPC and the ends of the VSD molecules proximal to the surface of the substrate contained within $25Å < z < 45Å$ in the profiles approaches 50% that of bulk aqueous buffer for $z > 80Å$. Exchange within the interior of the membrane is minimal, the level seen to arise from that within the interior of the VSD protein (red) for $45Å < z < 65Å$.

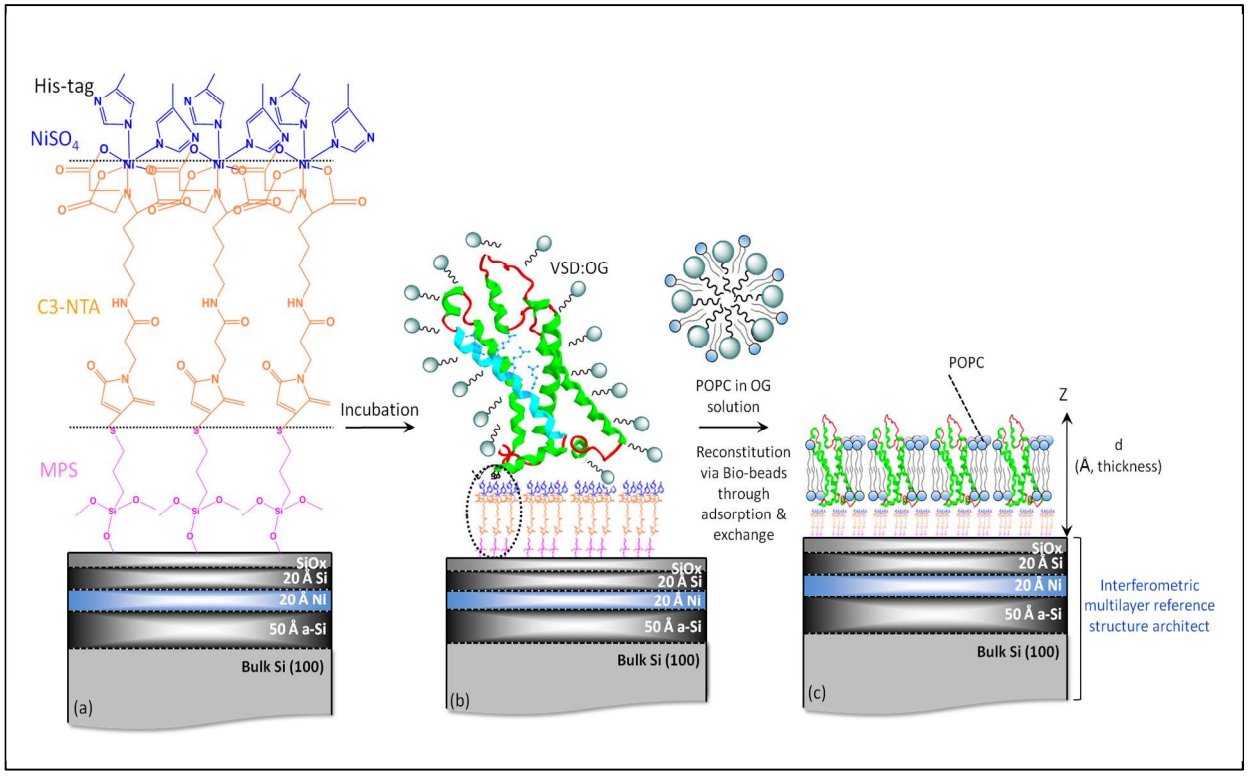

Figure S2: Schematic illustrating the SA approach adapted from reference [S1]. (a) A Si-Ni-Si (or SiGeSi) multilayer reference structure, alkylated with mercapto-propyl-silane [MPS] to functionalize its surface with thiol groups, is subsequently reacted with the linker maleimido–C_3-NTA to provide nitrilotriacetate endgroups for ligation with Ni^{+2} ions, along with (b) histidines from the protein's C-terminal His_6-tag following incubation with VSD:OG. (c) reconstitution of vectorially-oriented VSD in a single phospholipid bilayer environment via exchange against POPC/OG in the presence of Bio-beads. For aqueous environments, water is expected to partially hydrate the proximal side and fully hydrate the distal side (with respect to the substrate) of the reconstituted VSD:POPC membrane. The VSD is shown as ribbon representation of its crystal structure.

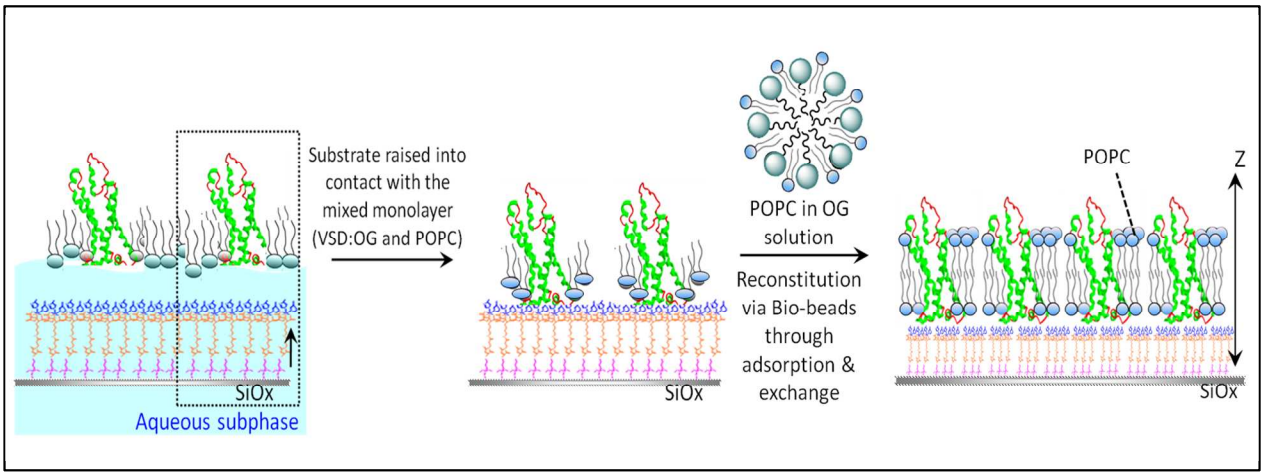

Figure S3: Schematic illustrating the DA approach adapted from reference [S1]. The lower surface of a sufficiently compressed (see text) Langmuir monolayer of a VSD/POPC mixture, containing VSD vectorially-oriented by its appended hydrophilic C-terminal sequence ending with a His_6-tag , is brought into contact with the upper surface of a Si-Ni-Si (or SiGeSi) multilayer substrate, alkylated to possess NTA endgroups ligating Ni^{+2} ions, shown in the left-to-middle frames. The resulting tethered VSD:POPC monolayer is subsequently exchanged against POPC/OG in the presence of Bio-beads & washed to reconstitute a POPC bilayer environment for the VSD, similar to that in the SA method illustrated in Figure S1.

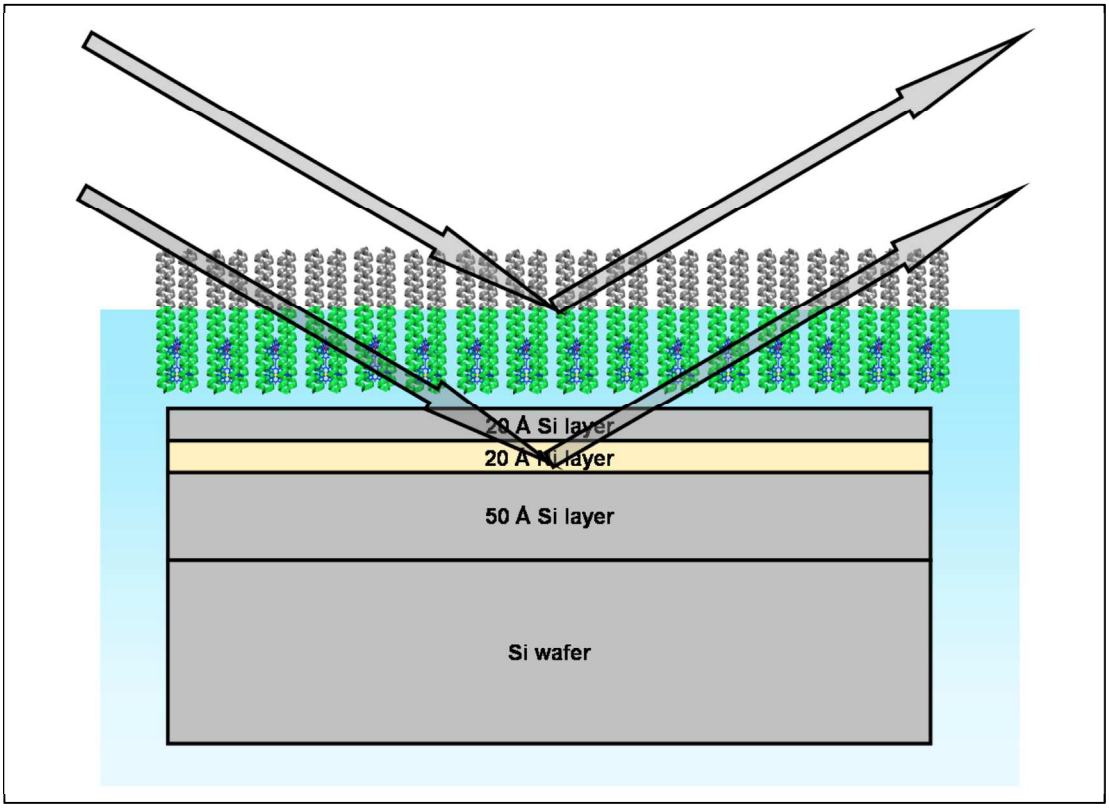

Figure S4: Schematic representation illustrating the interferometric approach to x-ray reflectivity to determine the profile structure of an ultrathin Langmuir film of a vectorially-oriented amphiphilic 4-helix bundle peptide (green & gray ribbon representation) containing a uniquely oriented chromophore (dark blue) at the liquid-gas interface. The sufficiently close proximity of the multilayer reference structure in the aqueous subphase (light blue) without contacting the otherwise unperturbed Langmuir monolayer of the amphiphile at the liquid-gas interface allows for the critical interference of x-rays reflected by the underlying reference structure (lower set of arrows denoting the directions of incident and elastically reflected photons) with those reflected by the monolayer of the amphiphile (upper set of arrows). Adapted from reference S4.

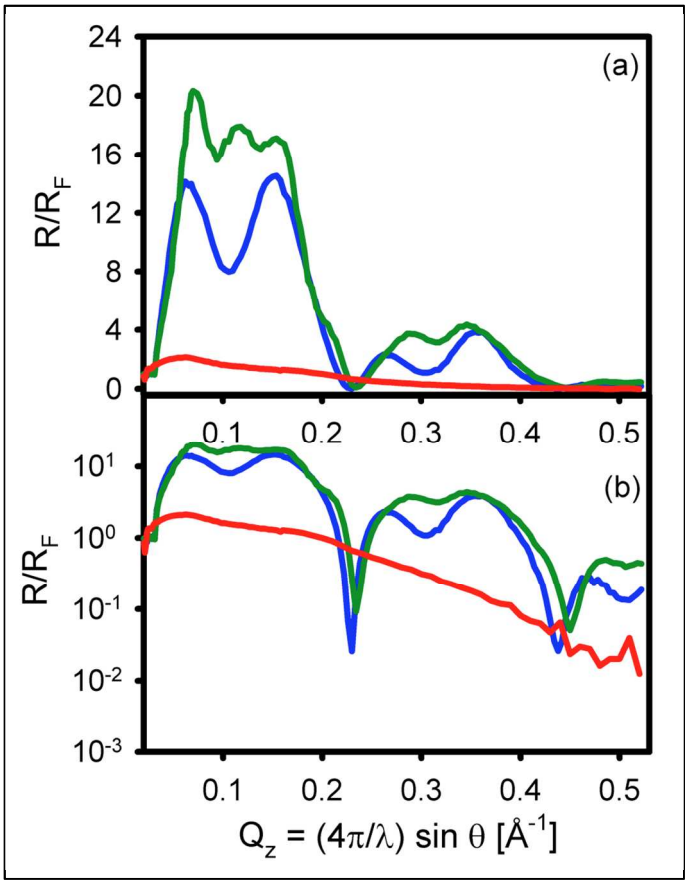

Figure S5: The Fresnel-normalized x-ray reflectivity (measured at 22.017 keV) from a Langmuir monolayer of the amphiphilic 4-helix bundle peptide, denoted AP0-RuPZn, obtained using either the non-interferometric or the interferometric approach shown along with that for the Si-Ni-Si multilayer reference structure itself, which possessed a macroscopically *hydrophobic* upper surface [blue curves: Si-Ni-Si reference structure itself in He, green curves: Langmuir monolayer of the amphiphile with the Si-Ni-Si reference structure positioned only slightly below in the aqueous subphase (interferometric case), and red curves: Langmuir monolayer of the amphiphile with the reference structure positioned far below the monolayer in the subphase (non-interferometric case)]. (a) Fresnel-normalized x-ray reflectivity data shown on a linear scale and (b) Fresnel normalized x-ray reflectivity data shown on a semi-logarithmic scale. The sensitivity of the x-ray (or neutron) reflectivity technique to the bio-organic monolayer is dramatically enhanced in the interferometric case, namely the *difference* between the green and blue curves, compared to the non-interferometric case (red curves). Adapted from reference S4.

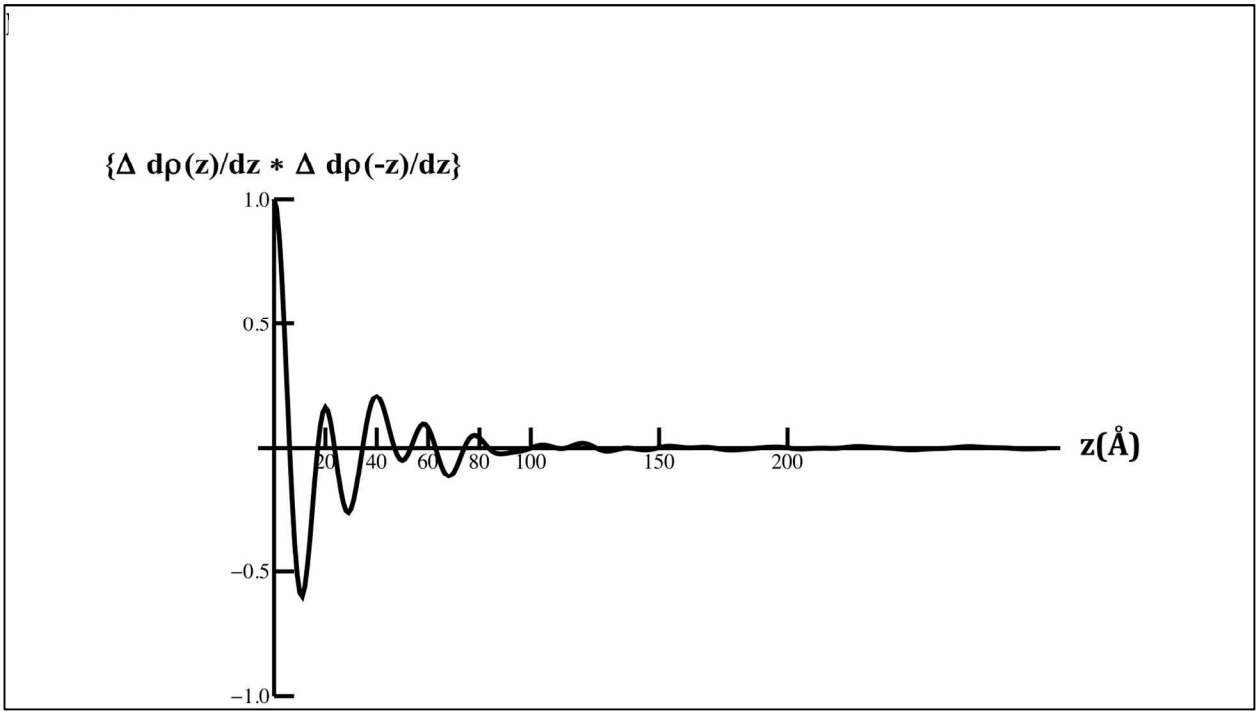

Figure S6: Autocorrelation function calculated from the *difference* modulus data for the VSD:POPC membrane for the potential pair {m100mV-0mV}. There are no significant fluctuations beyond z ~ 90Å, which thereby provides a key constraint for the box-refinement that determines the *difference* gradient profile $\Delta d\rho(z)/dz$ for the pair of potentials to within an overall sign.

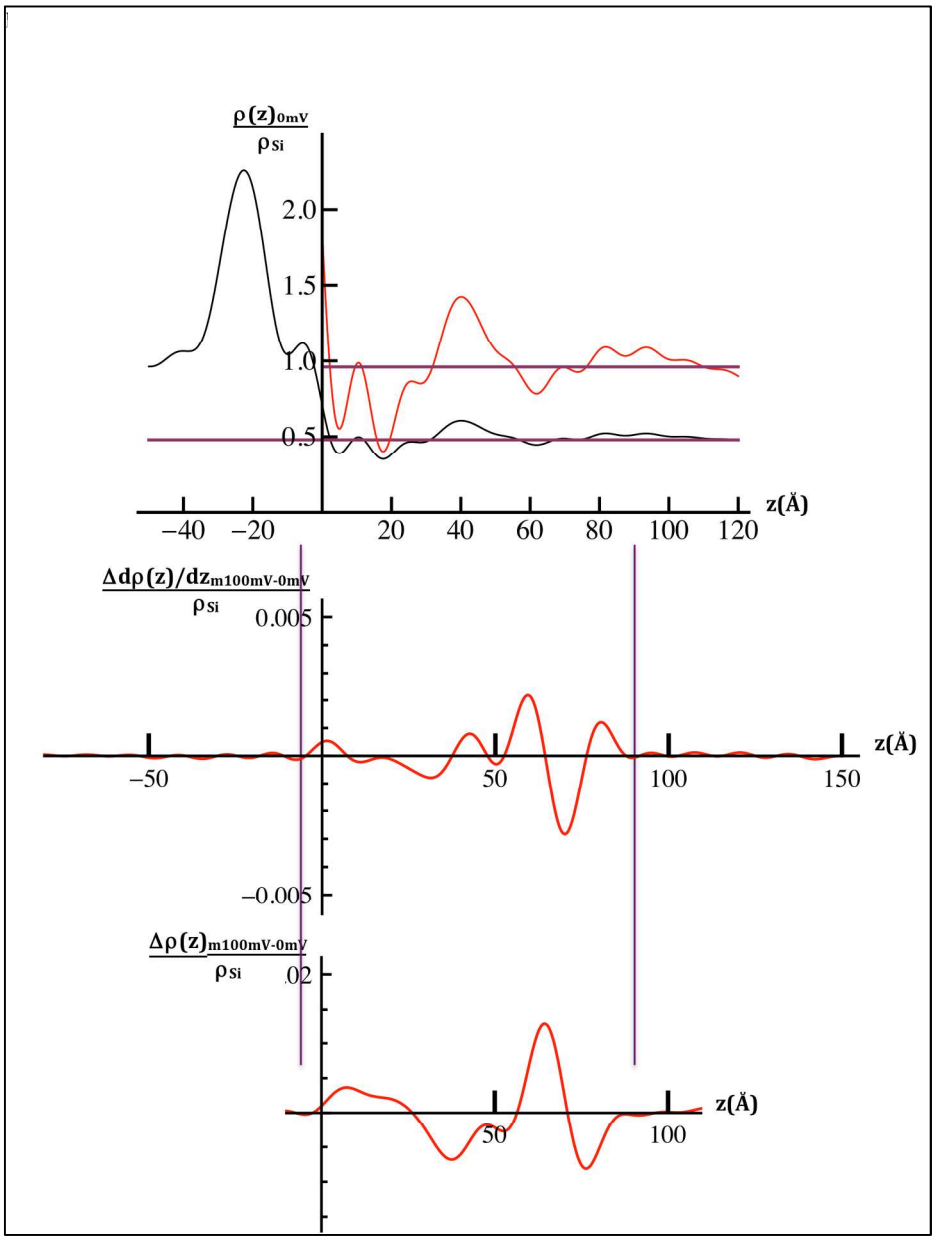

Figure S7: Upper: Reduced electron density profile for the VSD:POPC membrane tethered to the surface of a SiGeSi multilayer substrate at a transmembrane potential of 0mV. The tethered membrane appears within 0Å < z < 100Å while the substrate appears for z < 0Å, z = 0Å having been arbitrarily chosen as the origin of the profile z-axis, namely the surface of the substrate. The membrane region is also shown on an expanded and vertically-shifted ordinate-scale in red. Middle: The *difference* gradient profile $\Delta d\rho(z)/dz$ determined from box-refinement of the corresponding *difference* modulus data using slightly relaxed values of the constraint, namely 95-100Å. It clearly contains fluctuations only within the region bounded by -5Å < z < 90Å, indicated by the vertical magenta lines. The trial structure, whose phase function $\varphi(Q_z)$ was used to initiate the refinement, consisted of a single step-function of uniform non-zero electron density within the interval by 10Å < z < 70Å and zero otherwise for all potential pairs investigated. The integral of the *difference* gradient profile $\Delta d\rho(z)/dz$ providing the *difference* profile itself $\Delta\rho(z)/\rho_{Si}$, as shown in Figure 4 of the main text for the potential pair {m100mV-0mV}.

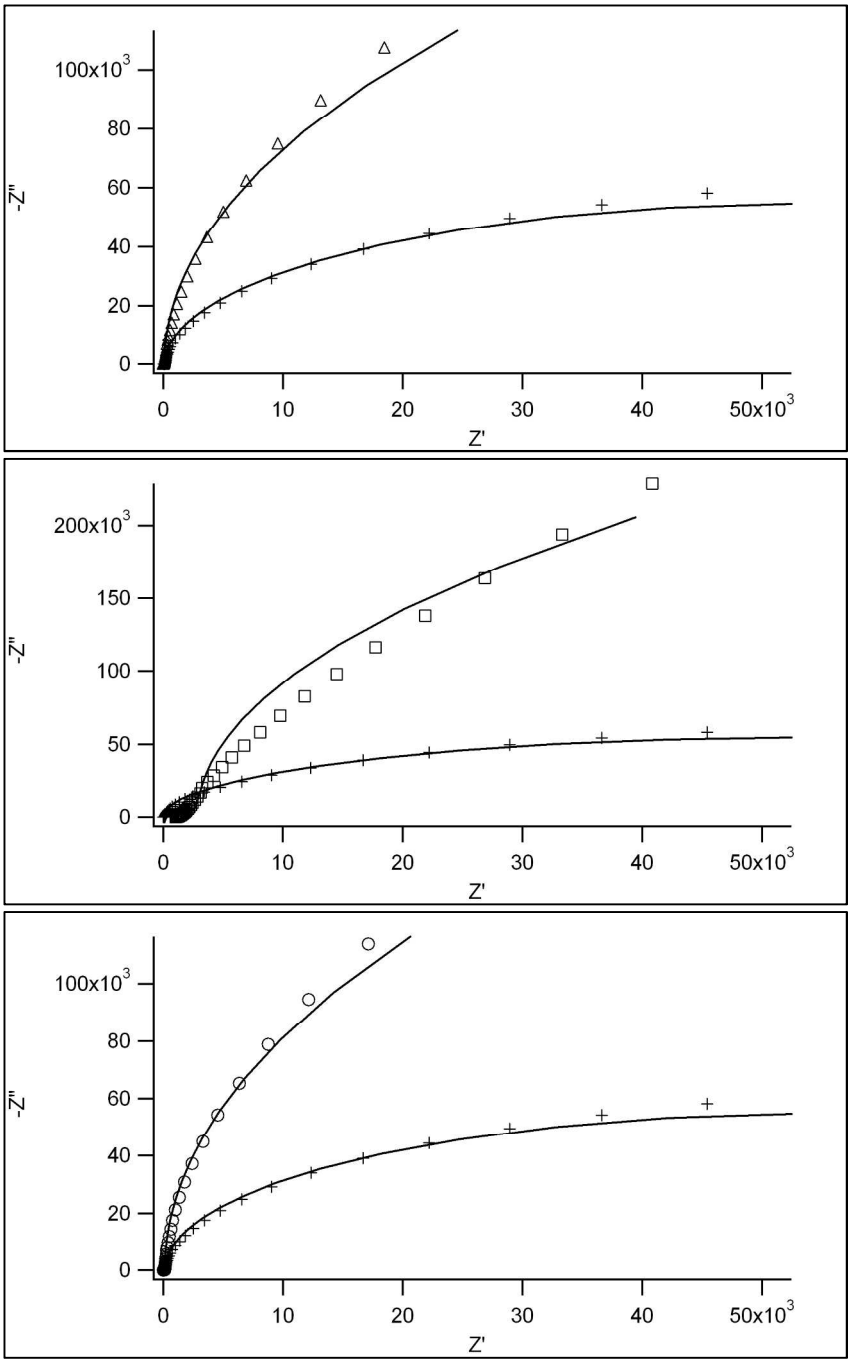

Figure S8: Nyquist plots of the electroimpedance spectra using the electrochemical cell employed in the time-resolved neutron interferometry experiments showing the frequency dependence of the real (Z') and imaginary (Z") parts of the impedance. Upper frame: Fits of the equivalent circuit model (see Experimental Methods) for the SiNiSi substrate (plus symbols; R= 360 ± 32 KΩ/cm^2, C=2.2 ± 0.2 μF/cm^2) and for the VSD:POPC membrane tethered to the surface of the SiNiSi substrate (triangles; R= 670 ± 60 KΩ/cm^2, C=1.8 ± 0.2 μF/cm^2). This particular specimen provided the time-resolved neutron interferometry data shown in Figure 5 in the main text. Middle frame: Fits of the equivalent circuit model for the SiNiSi substrate (plus symbols; R= 360 ± 32 KΩ/cm^2, C=2.2 ± 0.2 μF/cm^2) and for the hybrid OTS:POPC bilayer

tethered to the surface of the SiNiSi substrate (squares; R= 1.07 ± 0.05 MΩ/cm^2, C=0.6 ± 0.03 μF/cm^2). Lower frame: Fits of the equivalent circuit model for the SiNiSi substrate (plus symbols; R= 360 ± 32 KΩ/cm^2, C=2.2 ± 0.2 μF/cm^2) and for the SAM used to tether the VSD:POPC membrane to the surface of the SiNiSi substrate (circles; R= 1.5 ± 0.6 MΩ/cm^2, C=2.0 ± 0.1 μF/cm^2).